Etude d'un atome de Cesium dans une matrice d'argon pour des mesures fondamentales: moments dipolaire et anapolaire

Stage de M1 - Physique Fondamentale et Applications

Célia Smaï

Encadrants de stage: Daniel Comparat et Sebastian Lahs
Enseignant référent: Sophie Cribier

Sorbonne Université
Paris, France
Avril - Juillet 2023

Contents

1 Introduction

I did my intership at Laboratoire Aimé-Cotton (LAC), located in Orsay, is a joint research unit (UMR 9025) of the CNRS and the Université Paris-Saclay. It was created at the initiative of the famous physicist Aimé Cotton and it was inaugurated on July 9, 1928.
There are four different research groups called: THEOMOL (theory of cold molecule), MFC (Condensed Cold Matter), Nano^3 (Nanoparticles, Nanostructures and Nanomaterials) and HANDICAP (optronic sensors for the visually impaired). I had the opportunity to do my 3 months intership within the MFC group on the EDMMA experiment (electron dipole moment with atoms and molecules in a matrix) under the direction of Daniel Comparat (senior researcher) and Sebastian Lahs (PhD student). The system studied here is the cesium (Cs) atoms trapped in an argon (Ar) matrix.
During my intership, I worked on 2 different parts. First, I tried to find a new shape for the effective potential V_{Cs-Ar} between Cs and Ar that would give a better agreement between observed and simulated absorption line position. Then in a second part, I did studies to find out how a future measurement of the anapole moment of the nucleus could be performed.
All the work was done in the lab. I had access to a computer and I also helped with some manipulation to check the superconductivity of the coil that will be used later in the experiment.

2 eEDM measurements in cryogenic matrix

2.1 Context

The standard model (SM) is one of the most successful theories that describes all elementary particles and fundamental forces. However,the SM could not answer questions that arise from cosmological observations, such as the nature of dark matter and why matter dominates over antimatter throughout the Universe. There are some new theories that try to give answer to these problems by predicting new particles and introducing new sources of charge conjugaison (q $\rightarrow$ -q) -parity (r$\rightarrow$ -r) (CP) and time (t$\rightarrow$ -t) T violation. The validity of these theories can be checked by measuring fundamental properties like the electric dipole moment d_e of the electron and the anapole moment of the nucleus. For instance, the electron is a point charge, but when it interact with these new particles, it changes some of its properties and it appears as if it had an electric dipole moment.

For instance, up to now, the best non null measurement of electron EDM have been done in molecular beam (the current limit is $|d_e| < 10^{-30}$ e.cm). But the EDMMA project I worked on ambition to use alkali atoms embedded in noble-gas matrix. It has the potential to reach a statistical sensitivity in the order of 10^{-36}e.cm; a value several orders of magnitude beyond that of any other proposed technique, like atomic and molecular beams.
The measurement of the EDM is based on the shift $\Delta E = d_e.\mathcal{E}$ created when we apply an external electric field on the system. The statistical uncertainty of a single measurement is given through the Heisenberg time-energy uncertainty $\Delta E \Delta t \sim \hbar \implies \Delta d_e \sim \frac{\hbar}{\mathcal{E}\Delta t}$. For measurement on N independent atoms, it follows the Gaussian error propagation: $\Delta d_e = \frac{\hbar}{\mathcal{E}\Delta t\sqrt{N}}$. So if we want to improve the precision, we have to increase all the parameters and especially the number of particles and the coherence time Δt. With the EDMMA project that studies atoms trapped in solid matrix, it is possible to have bigger number of particles and longer coherence time than molecular beam that use dilute atoms in gas phase. As a first goal we plan $N \approx 10^{20}$, $\Delta t \sim 1\,\mathrm{s}$, $\mathcal{E} = 10^6 V/m$, with these values we expect to be able to reach a sensitivity for d_e around 10^{-30} e.cm.

2.2 Theoretical and experimental background

The system studied here is the Cs atoms trapped in an solidified argon matrix. An experimental and theoretical studies have been already done by the MFC team and preprinted (see ref.[1]). The transmission spectra was measured and compared with the simulation as shown in fig.1

In comparaison with the gaseous Cs, where only two dominant lines are present, the $6^2S_{1/2} \rightarrow 6^2P_{1/2}$ and the $6^2S_{1/2} \rightarrow 6^2P_{3/2}$ transition. The absorbance spectra of Cs embedded in Ar show two triplet structures.

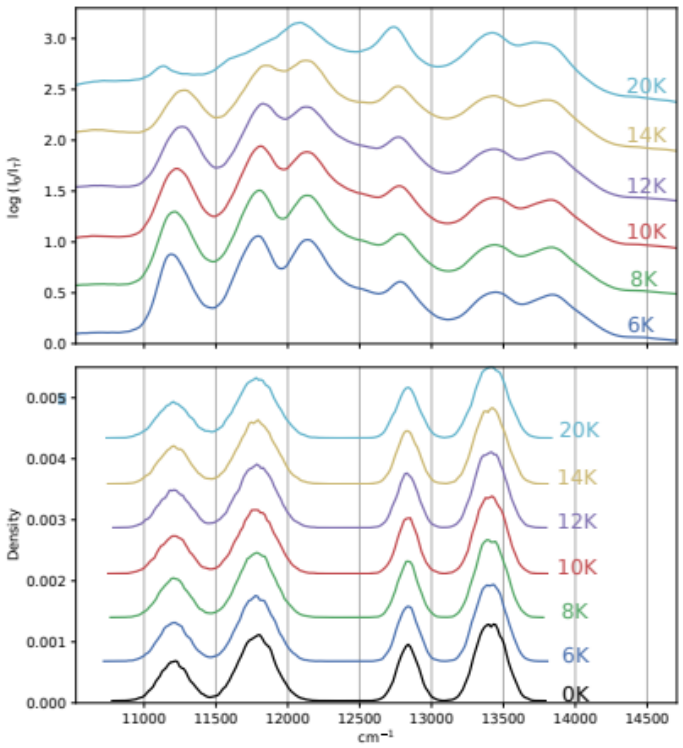

Figure 1: Comparaison between experimental absorption spectra (up) of Cs atoms embedded in a cryogenic Ar matrix and theoretical semi-classical Mulliken formula (bottom) at different temperatures T = 6 K,8 K,10 K,12 K, 14 K and 20 K and also for T = 0 K for the theory. For better visual clarity, vertical offsets have been applied to both the experimental and the theoretical spectra [1].

The doublet in gas phase $(P_{1/2}, P_{3/2})$ became a triplet in matrix. It is explained by the lift of degeneracy of the states $P_{3/2}$. The crystal field created by the surrounding Ar shifts the states according to the absolute value of the magnetic quantum number $|m|$, and so creating 3 lines: $P_{1/2} \rightarrow |m| = \frac{1}{2}$ and $P_{3/2} \rightarrow |m| = \frac{1}{2}, \frac{3}{2}$

The two structures visible in Fig.1 could be explained by 2 types of trapping sites inhabiting the crystal at once. In ref [1], the MFC team has proposed that they are due to a 4 vacancies tetrahedral T_d trapping site and to a 6 vacancies cubic O_h one for Cs atom in an Ar fcc matrix. An illustration of the geometry of these trapping sites is shown in fig.2

Figure 2: 4(left) and 6(right) vacancies trapping site of the Cs inside an fcc matrix of Ar (from [1]).

In order to reproduce numerically the triplet structure observed, a study laser excitation of the $6s$ Cs atom toward the $6p$ manifold was performed in [1]. In this study, the Cs-Ar is treated as a "big" molecules with $N \sim 1000$ atoms of Ar. To calculate the spectral density optical absorption coefficient $A(E)$ for a photon of energy E, several approximation have been used and the most important one is called the Mulliken approximation. It is given by:

$$A(E) \propto \int P_g(Q)\delta[E - (V_e(Q) - V_g(Q))]dQ$$

Q are the normal mode coordinates of the "big" molecules, $V_e(Q)$ is the electronical excited $6p$ potential energy curve and V_g is the ground state one. If $P_g(Q)$ is determined by classical statistics $P_g(Q) \propto e^{-V_g(Q)/k_bT}$, the formula is thus called classical. But if it is determined by the quantum-statistical mechanical probability distribution $|\Psi_i(Q)|^2$ of the ground state wave function occupied with probability P_i, then $P_g(Q) = \sum_i P_i|\Psi_i(Q)|^2$. We call it thus semi-classical.

The full interaction energy of a Cs doped crystal with $(N-n)$ Ar atoms and n vacancies is given by:
$V = \sum_{i=1}^{N-n} V_{Ar-Cs}(R_{Cs-Ar_i}) + \sum_{1\leq i\leq j\leq N-n} V_{Ar-Ar}(R_{ij})$. The full Ar-Ar and Cs-Ar interactions is calculated by using the two body pairwise potential approximation. we used $N \sim 1000$.

To perform the simulation, we use the pairewise potential Cs-Ar in the ground and excited state: without the spin-orbit interaction, the ground state is called $X\Sigma_{1/2}$ and it corresponds to the magnetic quantum number $|m| = 0$. Asymptotically at long range, we found that it corresponds to the state $6s$ of the Cs. For the excited state, it splits into two levels corresponding to $|m| = 1$ and $|m| = 0$, they are called respectively $A\Pi$ and $B\Sigma$. Asymptotically at long range, we found that it corresponds to the state $6p$ of the Cs.
The potential Π is attractive while the Σ one is repulsive (cf fig.3).

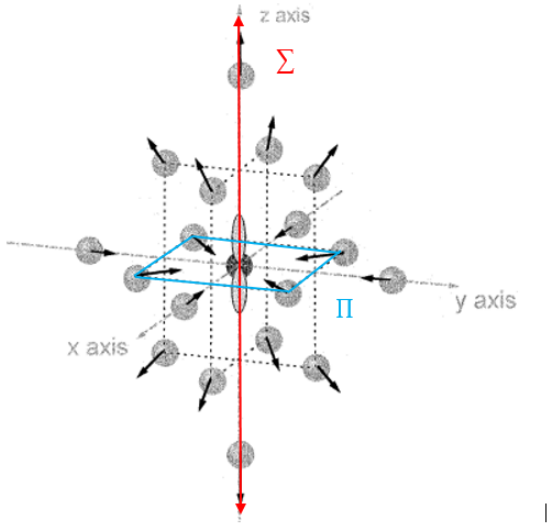

Figure 3: interaction between the Cs and the surrounding Ar[2].

In the sum of the full interaction energy, the pairwise potential depends on the position of the Ar atom relate to the Cs atom. For example, in the Fig.3 (taken from the article [2])the Cs in the center is in the state $6p_z$ ($|m| = 0$), when the Ar atoms are on the z axis, it induced a Σ interaction, when Ar is in the (xy) plane it's a Π interaction.

The integral $A(E)$ was calculated by using the Monte Carlo Method.

The comparaison with the experimental spectra (cf Fig.1) show that is clearly not sufficient. The theoretical absorption spectra does not give the triplet structure as in the experimental one.

In reality we have to consider the spin orbit interaction that will removes the degeneracy of the excited state : we will then have the $\Pi_{1/2}$ that gives the $6p_{1/2}$ at long range, and the two levels $\Pi_{3/2}$ and $\Sigma_{1/2}$ that gives the $6p_{3/2}$ level at long range.

2.3 Modification of the potential

The first part of my intership was to find numerically an effective potential $V_{B\Sigma} = V_{Cs-Ar}$ that would give a better agreement between observed and simulated absorption line position.

It is possible to modify the Σ state for two main reasons:

1- The pairwise potentials Cs-Ar are not well known, many potentials have been proposed in several articles from 1974 [3], 2012 [4], 2016 [5] and 2023 [6]. Let's note that the study in [1] was done before the one of 2023.
2- To compute the interaction potential of the Cs in the matrix of Ar, we use the two-body pairwise potential Cs-Ar over all atoms of Ar in the matrix. The effect of many-body correction has not been included. So the potential that we are looking for is a kind of effective potential that will take in consideration the many-body correction even if we still use the two body approximation.

First, I tried to do the calculation with the potential $B\Sigma$ of 1974 and 2023, because we already know that if we use the potential $B\Sigma$ of 2016 or 2012 the agreement with the experiment is not good(cf fig.1). Unfortunately it did not solve the problem.
Then, I tried to find which part of the potential should be modified to produce a triplet structure. I modified the potential at long range and at short range. In both case it did not work. After this, I did a substantial modification of the slope of the curve in the region of the nearest neighbors. In the O_h case, the first nearest neighbors Ar are at a distance of 0.465 nm of the Cs atom, the second at a distance of 5.923 nm and the third nearest neighbors at a distance of 7.965 nm. We found, that changing the slope of the curve around the position of the first nearest neighbors matters. Changing the potential in the region of the second and third nearest neighbors does not give the splitting. What is crucial is the slope between 0.44 nm and 0.48 nm. As an extreme modified potential $B\Sigma$ that gave a reasonable splitting for the T_d symmetries (4vacancies) is $V_{B\Sigma}^{modi}(r) = V_{B\Sigma}^{2016}(r) + 500\, e^{-(\frac{r-4.65}{0.39})^{10}}(\frac{r-4.65}{0.39})$ where r is in nm and $V_{B\Sigma}$ in cm^{-1}(cf fig.4).
The results of the simulation are shown in fig.5 and 6. When we compare with the experimental spectra (cf fig.1), the splitting looks good $\sim 1000\, cm^{-1}$ even if the total line position is still not good.

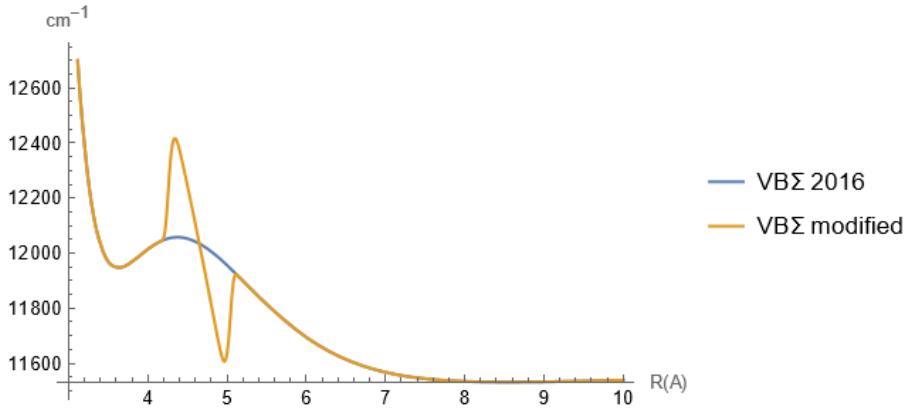

Figure 4: Comparaison between the original potential $B\Sigma$ of 2016 and the modified one $V_{B\Sigma}^{modi}$

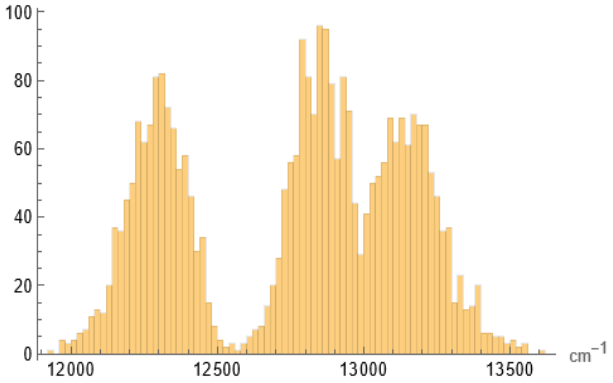

Figure 5: Spectrum for the O_h with $V_{B\Sigma}^{modi}$

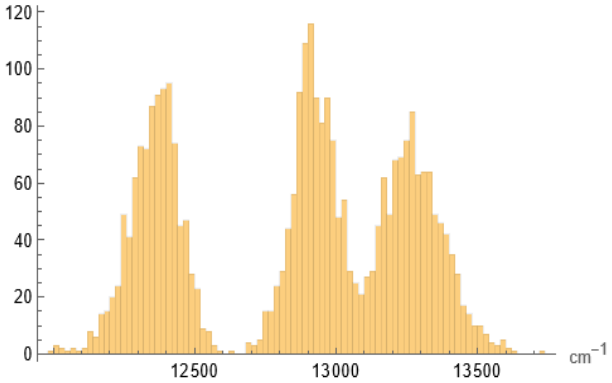

Figure 6: Spectrum for the T_d with $V_{B\Sigma}^{modi}$

We can see in fig.4 that it is not a "natural" shape for the potential, this is why we wanted to find a more natural and plausible one.
We know that theoretically, the potential at long range is proportional to $\frac{1}{r^6}$ because the Cs-Ar interaction is a Van Der Walls type of interaction. This is why we tried to find a potential in the form of $C_6(\frac{5}{r})^6 + C_8(\frac{5}{r})^8 + E(6p)$ which ensure the same slope in the region 0.44-0.48 nm, and the same potential at long range.
I was able to find different combination of (C_6, C_8) that fit very well with the spectrum of T_d, unfortunately not with O_h. We found $(C_6, C_8) = (-333, 514); (180, 400); (275, -14)$ in cm^{-1}. But thinking that the potential $B\Sigma$ is attractive, this suggests that C_6 should be negative.
In all these cases the spectra of O_h was shifted or the distance between the doublet was too small (cf fig 8 and 9).

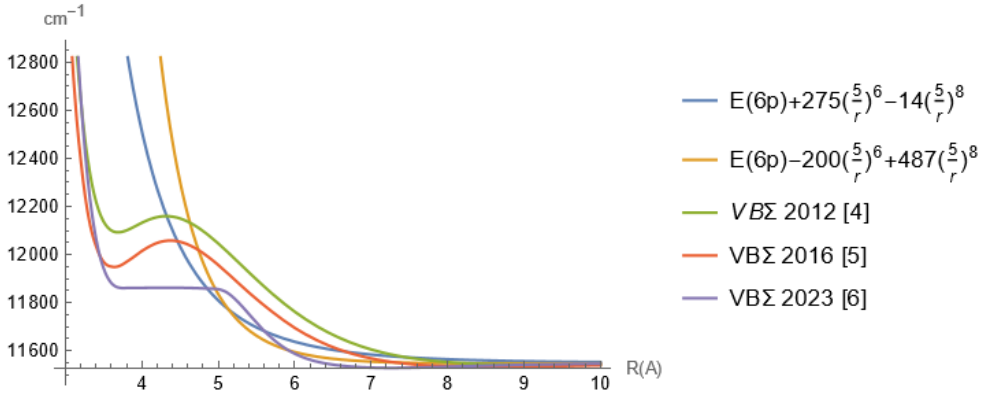

Figure 7: Comparaison between different BΣ potentials

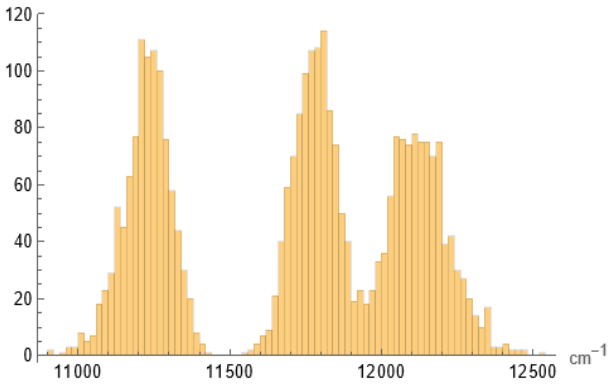

Figure 8: Spectrum for the T_d with $(C_6, C_8) = (-333, 514)$.

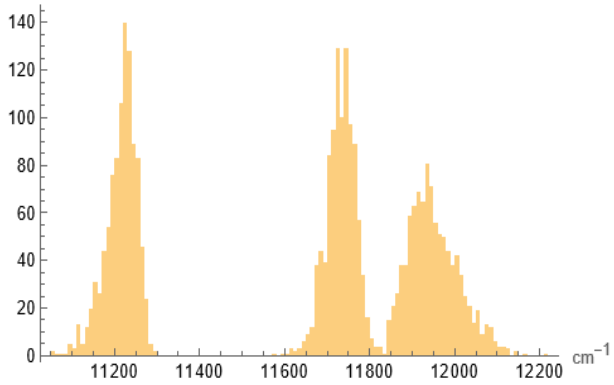

Figure 9: Spectrum for the O_h with $(C_6, C_8) = (-333, 514)$.

2.4 Conclusion

Even if we were able to obtain the triplet structure in both T_d and O_h the positions lines are still not good. What could explain the discrepancy between the experiment and simulation is that we did not find the good trapping site of the Cs in the matrix of Ar. It has been showed since the 70th that in addition to the Ar being in an fcc matrix, it can be also in an hcp phase. This can leads to a 5 vacancies trapping site for Cs in *hcp* matrix of Ar. So we could have either a 4 (in fcc matrix) and 5 (in *hcp* matrix) vacancies trapping site or a 6 (in fcc matrix) and 5 (in *hcp* matrix) vacancies trapping site.

3 Anapole moment

The anapole moment of the nucleus is a parity violating nuclear property that comes from the weak interaction. It can be described as a type of electromagnetic multiple moment that characterizes the distribution of electric currents in the nucleus. It was measured only one time in 1997 on a beam of Cs and it was difficult to perform.
It is interesting to measure the anapole moment of a nucleus because it provides valuable information about nuclear system, fundamental interaction, especially the weak interaction and its effects on nuclear processes, parity violation and potentially dark matter detection. This knowledge can help us understand the behavior of matter at the sub-atomic level and contribute to our understanding of the universe.

In the article [7], it was shown that the anapole manifests in system with anisotropy, like the case of ground state Cs atoms trapped in uniaxial symmetry *hcp* matrix of Ar, as a linear stark shift. So we hope that indeed we have in our system an *hcp* matrix of Ar with 5 vacancies because the anisotropy cannot be created in the T_d and O_h case. In this section, studies for our particular system are presented to find out how a future measurement could be performed.

3.1 Hamiltonian of the system

The hamiltonian of the Cs inside the matrix of Ar in the presence of an applied electric and magnetic field is given by:

$$H = (H_{at} + H_{CF}) + H_{hyperfine} + H_{zeeman} + H_{spin-orbit} + H_{anapole}$$

H_{at} is the hamiltonian of the Cs in the gas phase, the eigenstates are given by the wave function $|nlm\rangle$. When we add the crystal field to H_{at}, the new eigenstate becomes $|\tilde{nlm}\rangle$. Using the other terms and the perturbation theory with the new basis $|\tilde{nlm}\rangle$, we find the effective hamiltonian with a given $|\tilde{nl}\rangle$ manifold. For the ground state $|\tilde{6s}\rangle$ we have:

$$\begin{aligned} H_{eff} &= H^{eff}_{hyperfine} + H^{eff}_{zeeman} + H_{anapole} \\ &= S.A.I + (g_s \mu_B S.B + g_I \mu_B I.B) + d_I (S \wedge I) E_{ext} \end{aligned}$$

Where μ_B is the Bohr magneton, d_I the anapole, g_s the Landé factor of the electron and g_I the Landé factor of the nucleus.
It was shown that depending on the trapping site of the Cs, an anistropy can be created and it is manifested by the hyperfine constant A that become a tensor. It happens when the Cs is trapped in a matrix of Ar having an hexagonal symmetry.

At low magnetic field, the dominant term is the hyperfine structure one, the good basis is hence $|F, m_F\rangle$ with $\boldsymbol{F} = \boldsymbol{I} + \boldsymbol{S}$, all other terms (zeeman, and anapole) are considered as a perturbation.
On the contrary, if we are at high magnetic field, the dominant term is the Zeeman one and the good basis is then $|s, m_S, I, m_I\rangle$.

The energy levels of the Cs in its ground state are given by fig 10.

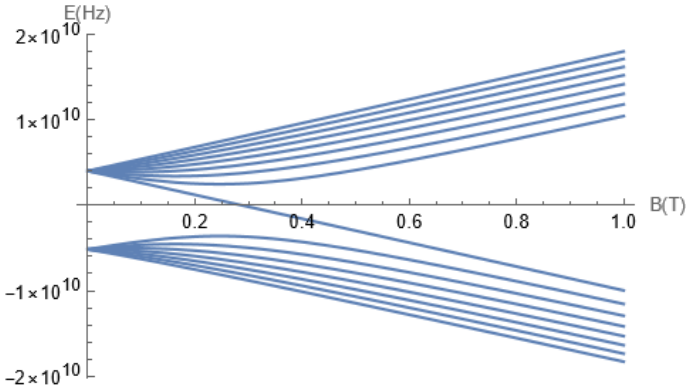

Figure 10: Energy levels of ground state Cs trapped in an *hcp* matrix of Ar.

To see the effect of the anisotropy we did a zoom on the plot above in the limit of low magnetic field. In the plot below, we put an offset to be able to see the lift of degeneracy of all the states concerned in the same figure.

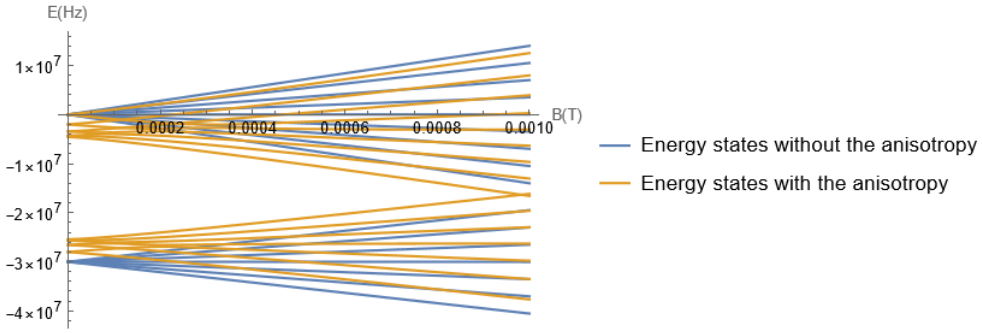

Figure 11: Comparaison between the energy level of the Cs in its ground state with and without the anisotropy. We put an offset to be able to see the lift of degeneracy of all the states concerned in the same figure.

We can see from this plot that the anisotropy removes the degeneracy at B=0. Theoretically we can show that at B=0, the energy level depends on m_F^2.

3.2 Symmetry consideration

In order to be able to measure the energy shift created by the anapole we should have a nonzero linear stark shift. It was mentioned but not clearly demonstrated in [7], that this can be achieved by perturbating the atomic ground state with a crystal field compatible wih uniaxial symmetry along the unit vector **n**. I propose here a demonstration of this:

For reasons of simplicity, we suppose that the magnetic field **B** is along the **z** axis and the electric field **E** along the

y axis. The Stark hamiltonian can be written then as: $H_{anapole} = d_I(s \wedge I)E_{ext} = d_I(s_z I_x - s_x I_z)E_y$.

Let's consider the symmetry $\hat{\Theta} = \hat{T}\hat{R}(\hat{e_x}, \pi)$ where $\hat{T}$ is the time reversal operator and $\hat{R}(\hat{\mathbf{u}}, \pi)$ is rotation of π around the unit vector $\boldsymbol{u} = \boldsymbol{e_x}$.

We can note that $\hat{\Theta}$ is an antiunitary operator, so we have $\hat{\Theta}^\dagger = \hat{\Theta}^{-1}$. The two operators $\hat{\Theta}$ and $\hat{R}$ act only on the spin states. Here the external field B and E are considered as real numbers and are not affected.
Here a summary of how act the $\hat{\Theta}$ operator on the electronic and nuclear spin.

Quantity	Rotation $\hat{R}(\hat{\mathbf{x}}, \pi)$	Time reversal $\hat{T}$	$\hat{\Theta}$
s_x, I_x	+	-	-
$s_{y,z}, I_{y,z}$	-	-	+
$\boldsymbol{E}, \boldsymbol{B}$	+	+	+

We can see from the table above that $H^{eff}_{zeeman} = g_s\mu_B S.B + g_I\mu_B I.B$ is invariant under the symmetry $\hat{\Theta}$, which means $\hat{\Theta}$ and H^{eff}_{zeeman} have the same eigensate $\hat{\Theta}$: $\hat{\Theta}|\psi\rangle = |\psi\rangle$
Concerning $H_{anapole}$, it changes sign, which means $\hat{\Theta}^{-1}H_{anapole}\hat{\Theta} = -H_{anapole}$.

To determine the linear stark shift due to the anapole, we apply the theory of perturbation at the first order:

$$\begin{aligned}\Delta E^{Stark} &= \langle\psi|H_{anapole}|\psi\rangle = \langle\psi|\hat{\Theta}^\dagger\hat{\Theta}H_{anapole}\hat{\Theta}^{-1}\hat{\Theta}|\psi\rangle \\ &= \langle\psi|\hat{\Theta}H_{anapole}\hat{\Theta}^{-1}|\psi\rangle = -\langle\psi|H_{anapole}|\psi\rangle \\ &= -\Delta E^{Stark}\end{aligned}$$

From this we can conclude that $\Delta E^{Stark} = 0$ if A is a constant. So, in order to suppress the linear Stark shift cancellation we have to break the $\hat{\Theta}$ symmetry ($\hat{\Theta}|\psi\rangle \neq |\psi\rangle$). For instance by introducing an anistropic hyperfine interaction by perturbating the atomic ground sate $S_{1/2}$ with a crystal field compatible with uniaxial symmetry along a unit vector $\boldsymbol{n}$. The new ground state $|\tilde{6s}\rangle$ will be a mixture of S and D state. The new spin hamiltonian reads [7]:

$$\tilde{H}_{spin} = A_\perp s.I + (A_{||} - A_\perp)(s.n)(I.n) + g_s\mu_B S.B + g_I\mu_B I.B)$$

The axis of the crystal **n** is caracterized by its spherical angles θ and ϕ.

3.3 Numerical study of crystal anisotropy and magnetic field

To have a better understanding of how the Stark shift varies as a function of **B**, I did a numerical study with Mathematica. A code has already been written with the effective Hamiltonian. First I had to understand it well before I could use it. To take in consideration the anistropy, A is a tensor that depends on $\epsilon = \frac{A_{||} - A_\perp}{A_\perp}$ and also on the angle θ and ϕ due to the fact that we have a polycrystal.
To obtain the energies corresponding to each state, we diagonalized the effective hamiltonian in the basis $|m_s, m_I\rangle$. Because $I = \frac{7}{2}$ and $s = \frac{1}{2}$, we have then to calculate the eigenvalues of a 16×16 matrix (16=(2I+1)(2s+1)). For the simulation, we choose $\epsilon = 0.001$ (ref [7]), and fix the electric field to $E = 10^6$ V/m (reasonable value). For numerical reasons (to remove the numerical noise in Mathematica) we artificially increase by 10^6 the anapole value. Below $10^5 d_{I0}$ we start to get numerical noise, and greater than $10^7 d_{I0}$, $H_{anapole}$ is not anymore a perturbation and we get wrong results.

At the beginning, we wanted to know which angles (θ, ϕ) maximize the shift. First we did it analytically in the limit of strong magnetic field.
From the Bouchiat and Bouchiat paper [7], the linear stark shift in the strong limit of B is proportional to $\frac{(\boldsymbol{n.B})\boldsymbol{n}.(\boldsymbol{E}\times\boldsymbol{B})}{B^2}$.
In spherical coordinates, we write **n** as $\begin{pmatrix} sin\theta cos\phi \\ sin\theta sin\phi \\ cos\theta \end{pmatrix}$. We are always in the case where **B** is along **z** and **E** along **y**. The Stark shift is hence proportional to $Ecos\theta sin\theta cos\phi = \frac{1}{2}sin(2\theta)cos\phi$. It's a function of two separable variables that reach its maximum when $sin(2\theta)$ and $cos\phi$ are at their maximum. So we find $\theta_{max} = \frac{\pi}{4}, \frac{3\pi}{4}$ and $\phi_{max} = 0, \pi$.

We have checked this numerically. For this We fixed at the beginning ϕ to 0 and plotted the Stark shift as a function of θ, we found the same θ_{max} as theoretically (fig 12). We fixed θ to $\frac{\pi}{4}$ and plotted the linear Stark shift as a function of ϕ (fig 13). We found the same $(\theta, \phi)_{max}$ at low magnetic field.

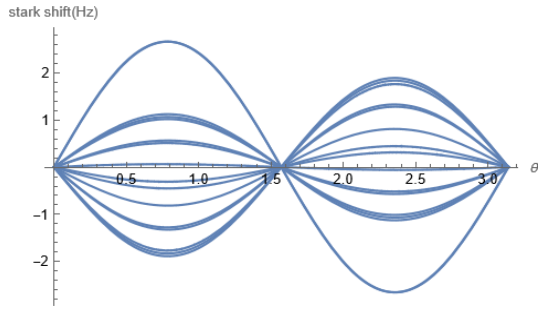

Figure 12: variation of the stark shift of the 16 ground state level depending on the angle θ when B=0.25 T

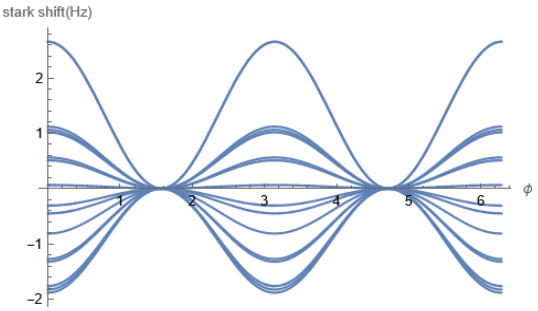

Figure 13: variation of the stark shift of the 16 ground state level depending on the angle ϕ when B=0.25 T

Knowing that we have a polycrystal, we have to average on the angles θ and ϕ to be more realistic. We struggled numerically to calculate the average, so we plot instead a histogram of the distribution of anapole-induced energy shifts in a polycrystal. We choose 10^5 directions for $\mathbf{n}$ to span the whole space.

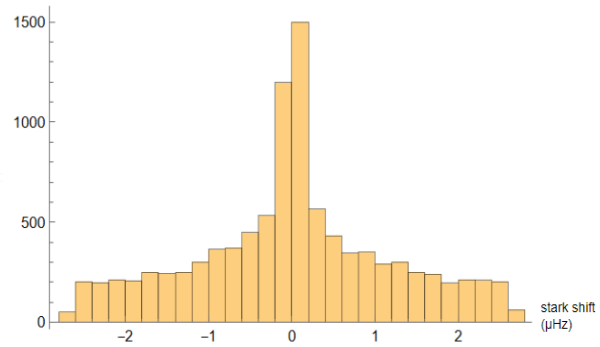

Figure 14: Histogram of the distribution of anapole induced energy shifts in polycrystal with B=1 T and E=10^6 V/m for the level $|4, 4\rangle$

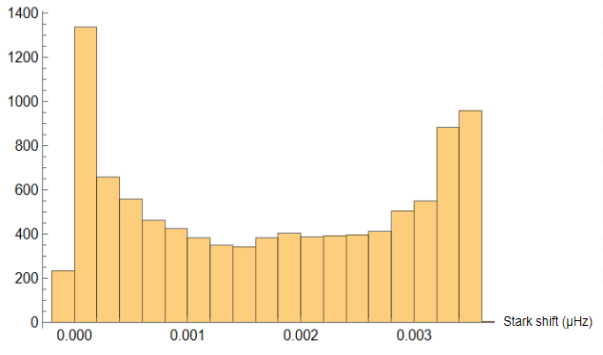

Figure 15: Histogram of the distribution of anapole induced energy shifts in polycrystal with B=10^{-6} T and E=10^6 V/m for the level $|4, 4\rangle$

We can see that the energy shift average is of the order of μHz (Fig.14) at strong magnetic field, and in the order of nHz at low magnetic field (Fig.15). μHz seems a measurable shift because state of the art magnetometer energy resolution are in the fT regime and a Zeeman shift is on the order of few GHz/T. But clearly a more detail study is needed. So I study the effect on the instability of the magnetic field $\boldsymbol{B}$.

3.4 Study of effect on the instability of the magnetic field $\boldsymbol{B}$

To do a measurement of the anapole, we measure first the energy transition $\Delta E(B, \mathcal{E})_{ij} = E(B, \mathcal{E})_j - E(B, \mathcal{E})_i$ between two levels i and j at zero external electric field $\mathcal{E}$. Then we add the electric field $\mathcal{E} = 10^6$ V/m and measure again the energy transition. The difference between them will give us the linear Stark shift due to the anapole.

To create the external magnetic field B, we use a current in a coil. The instability of the current turn into an incertitude ΔB in the B field. This incertitude is estimated by the reasonable value $\Delta B = 10^{-5} B$. It can create a noise that can be greater than the Stark shift induced by the anapole.

We thus need to study this more carefully. To be able to measure the anapole, the noise that come from the instability of the magnetic field should be smaller than the linear Stark shift. The best will be to use a transition where the shift is independent of B.
We want to compare this noise that we roughly estimate by $E_{noise} = \Delta E(B + \Delta B, \mathcal{E})_{ij} - \Delta E(B, \mathcal{E})_{ij}$ to the energy Stark shift induced by the anapole $E^{anapole} = |\Delta E(B, \mathcal{E})_{ij} - \Delta E(B, 0))_{ij}|$. we used $\Delta B = 10^{-5} B$ and $(\theta, \phi) = (\frac{\pi}{4}, 0)$. For this we plotted the ratio $\frac{E^{anapole}}{E_{noise}}$ for all the transitions $i \to j$ and looked for the cases where it is greater 1. But, the value is typically in the the order of 10^{-5}.
The only transition that was not too bad is the transition $|4, -4\rangle \to |4, -3\rangle$, here $\frac{E^{anapole}}{E_{noise}}$ was in the order 10^{-1} for B=4.6 μT. To have a ratio greater than 1, the relative error $\frac{\Delta B}{B} = 10^{-5}$ was maybe pessimistic. Some group research have currently reached in their experiemnts $\frac{\Delta B}{B} = 10^{-9}$. This may solve our problem by bringing $\frac{E^{anapole}}{E_{noise}}$ to a value well above 1. However $\frac{E^{anapole}}{E_{noise}}$ is not the only parameter because $E^{anapole}$ should be measurable and so be in the μHz range.

3.5 Different regimes

We plot the linear Stark shift $E(B, \mathcal{E})_i - E(B, 0)_i$ for each state i as a function of B to understand better how it varies. We used the semi log scale and vary B 10^{-6} to 10 T.The result is given by fig 16.

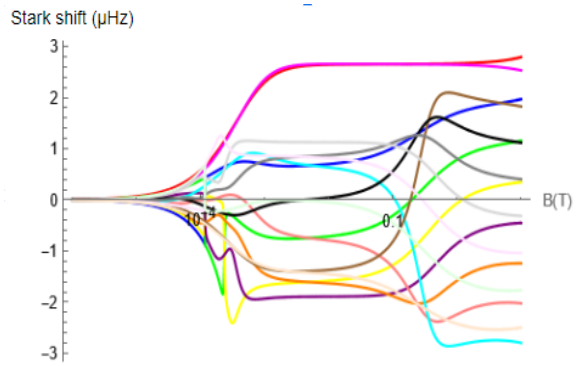

Figure 16: Variation of the linear stark shift depending on the magnetic field in a semilog scale

A numerical problem is that when two energy states cross, it inverts the color of the two curves. Despite this, we can recognize the different regimes discussed in the Bouchiat and Bouchiat paper [7]. The first one is the strong magnetic field limit when $\mu_B g_s B \gg A_\perp \gg |A_{||} - A_\perp|$, in other terms when $H_{zeeman} \gg H_{hf}^{isotropic} \gg H_{hf}^{anisotropic}$. From the fig. 16, we see that it corrsponds to $B > 1$ T. The second regime is the intermediate one when $A_\perp \gg \mu_B g_s B \gg |A_{||} - A_\perp|$. It corresponds to $1\,mT < B < 0.1$ T. In [7], three main properties have been shown in these two regimes that we confirm more precisely: the linear Stark Shift is proportional to the anisotropy $\frac{A_{||} - A_\perp}{A_{||} + A_\perp}$, it is independent of $|\mathbf{B}|$ and it depends only on the direction of $\mathbf{B}$.
We can also note from the plot that at low magnetic field ($B < 1\,mT$), the stark shift is linear with B. In this case $A_\perp \gg |A_\perp - A_{||}| \gg \mu_B g_s B$. In the special case where the magnetic field is null, the stark shift is null also. This result is a big problem because as shown in the previous study, low magnetic field is needed to have the anapole effect bigger than the noise.
We can give a simple explanation of the fact that $E_{anapole} = 0$ for B=0 with the projection theorem, a special case of the Wigner-Eckart theorem.
It says that in $|F, m\rangle$ manifold, a vector $\boldsymbol{V}$ can be replaced by its projection on $\boldsymbol{F}$, its expression is given by: $\boldsymbol{V} = \frac{\boldsymbol{V}.\boldsymbol{J}}{|\boldsymbol{J^2}|}\boldsymbol{J}$. In other terms, any vector operator can be seen as precessing around the total angular momentum $\boldsymbol{F}$, and the average value of $\boldsymbol{V}$ is the projection of $\boldsymbol{V}$ on $\boldsymbol{F}$. In fig.17, we use this at B=0 for $\boldsymbol{s}$ and $\boldsymbol{I}$ to show that $\boldsymbol{s}$ and $\boldsymbol{I}$ are aligned and so $H_{anapole} = d_I(S \wedge I)E_{ext} = 0$.

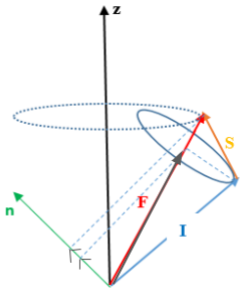

Figure 17: Projection theorem. When B=0, the hamiltonian is written as $H = A_\perp \boldsymbol{s}.\boldsymbol{I} + (A_{||} - A_\perp)(\boldsymbol{s}.\boldsymbol{n})(\boldsymbol{I}.\boldsymbol{n}) + H_{anapole}$ with $A_\perp \gg |A_{||} - A_\perp|$. The first term implies that what matters is the projection of $\boldsymbol{s}$ and $\boldsymbol{I}$ on $\boldsymbol{F}$, it's like if they were aligned. The anisotropy term will tend to project $\boldsymbol{s}$ and $\boldsymbol{I}$ on $\boldsymbol{n}$. Here $\boldsymbol{s}$ and $\boldsymbol{I}$ play the same role and will change a bit $\boldsymbol{s}$ and $\boldsymbol{I}$ but in the same way. So they stay aligned. Thus, $H_{anapole} = d_I(S \wedge I)E_{ext} = 0$.

A theoretical study is currently in progress to properly study this limit and see if there is a a way to go around it and get nonzero shift. The first step is to write the hamiltonian in the more appropriate basis $|F, m_F\rangle$ in low magnetic field. For this we need to find the change-of-basis matrix P from the old basis $|s, m_s, I, m_I\rangle$ to the new one $|F, m_F\rangle$. I did it with mathematica by calculating the Clebsh Gordan. Then the next step is to write the term $A_\perp \boldsymbol{s}.\boldsymbol{I}$ of the hamiltonian in the new basis. We obtain a diagonal matrix. We treat the anisotropy as perturbation at the first order in the degenerate case.We will still have the same eigenstates but different energies. After this, we should apply again the theory of perturbation on H_{zeeman}, it will change the eigenstates to $|F, \tilde{m}_F\rangle$ and then on $H_{anapole}$. This work is still in progress.

3.6 conclusion

From the above studies we can see that what makes the measurement of the anapole hard is that at strong magnetic field the noise induced by the instability of B is too big comparing to the shift induced by the anapole. At low magnetic field the anapole induced Stark shift is too small to do any measurement.
Our current strategy to solve these problems are the following. First, we can work at the lowest possible magnetic field where the anapole stil play a role so in the region $B \sim 1$ mT. Second, to work at low B field but to try to restore the effect of the anapole. What can try to do this by considering the fact that g_s could be a tensor due to an anisotropy of the crystal. This comes from the fact that the anisotropic electron orbit will affect the zeeman hamiltonian throught spin-orbit interaction. Another possibility is to change the direction of the electric field, it would have two component E_x and E_y. A first try showed that it does not change anything but further investigation should be done. Indeed, we have neglected the classique Stark hamiltonian in the effective hamiltonian. Adding this term may increase the stark shift induced by the anapole.

4 Superconductivity of the coil

Beside the computational work, I worked also on the experiment by checking the superconductivity of the coil that will be used later to create an external magnetic field. For this, we varied the intensity and we measured the tension and the temperature. Even if at the end, we did not succeed to obtain a a superconductive coil, I learnt how a cryostat work and the procedure to follow to try to find a solution to our problem.

4.1 The necessary setup to solidify the argon

The cryostat used in this experiment was manufactured by *Mycrofirm* and can operate down to 3.3 K. It consists of two cooling stages, that are enclosed in copper shields plated with gold. We use two shields to protect from black body radiation. The copper is used for its property of being a good thermal conductor, and the gold is used to reflect the radiation. The first shield is at 50 K and the second one at 4 K. The Fig.18 shows the experimental setup inside the 4 K shield.
The heat in the setup is pumped out by a cryocooler. It uses a circuit system of liquid helium that cools down by

expansion.
To vacuum inside is created by two pumps called the scroll pump and the turbo molecular pump. The first one is used to pump 1 Pa, and the second one it used to pump from 1 Pa to 10^{-5} Pa.

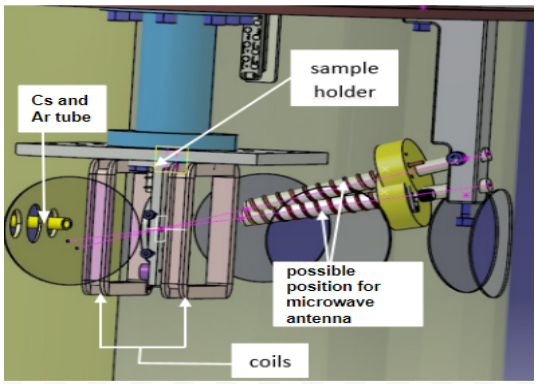

Figure 18: Experimental setup inside the 4 K shield.

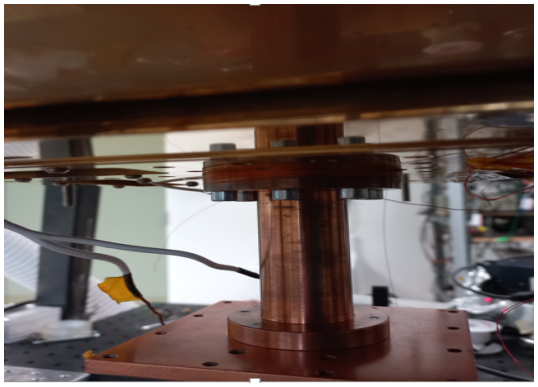

Figure 19: Close picture of the sample holder and the coil inside the 4 K shield.

4.2 Experimental results

To check the superconductivity of the coil, we plot its resistivity as a function of the current in order to find its critical current below which the resistance is quasi null and constant. We were supposed to find the critical current around 20 A, but the measurement shown in Fig.20 indicates that it is around 1.5 A. The coil is not super conductive.

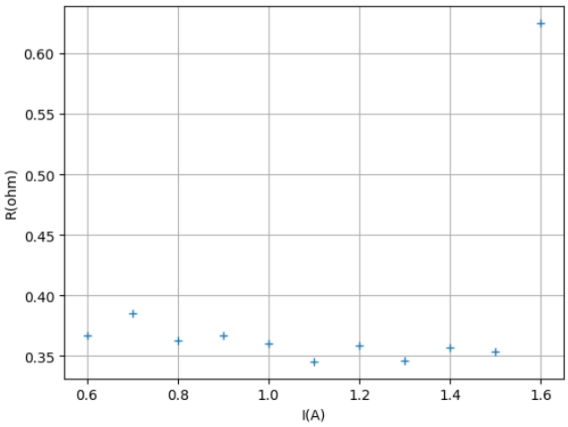

Figure 20: Variation of the resistivity of the coil depending on the current. 0.35 Ω is an offset due to the fact that the big wire that connects the generator with the coil is not superconductive.

We did many hypothesis and test to find out where is the problem but we could not fix it.
1- At the beginning, we thought that maybe there was a broken point in the wire that heat up and then heat all the coils.
2- After this, we checked if the connection between the wire and the high temperature superconductive wire that is used to connected to the external generator of current does not heat up. It turned out that it is not the case.
3- We use only one simpler coil to have a better understanding of what happened.
4- The first coils holder was made of Brass, we changed it with copper in order to have better thermal contact.
5- We changed the location of the coil and put it in contact with the 4 K shield and hence be sure that there is a good thermal contact (cf Fig.19).
6- We pay attention to not have floating wire for 2 reasons: first the magnetic force will move them and create a huge tension and can lead to removing the superconductivity, second it is in a bad thermal contact if it is in vacuum.

After all this tries we were not able to have a superconductive coil. The next step is to ask more advice to an expert.

5 Conclusion

5.1 Summary and perspective

In summary, in the first work on the modification of the potential gave a good agreement between the experimental and the simulated absorption spectrum for the T_d case but not for the O_h case. So from the work done by the MFC group and the results of the modification of the potential $V_{B\Sigma}$, we arrive to the conclusion that this discrepancy can be explained by another possible trapping site for the Cs in Ar matrix. Indeed, We used only the fact that the Ar crystallize in an fcc phase which gives the 4 and 6 vacancies. But It was shown recently that it can also crystallized in an *hcp* phase which lead to a 5 vacancy trapping site. This is a good lead for future investigations.
Concerning the measurement of the anapole moment of the nucleus, we are facing to two main problems. The study done here showed that if we do the measurement for values of magnetic field B greater than 1 mT, the noise introduced by the instability of the B is greater than the stark shift induced by the anapole. If we work at low magnetic field, the shift induced by the anapole can quickly become too small (in the order of nHz) and being non detectable by using the current technology. The strategy now is to study theoretically how vary the shift induced by the anapole at low magnetic $B \sim 1\,\mathrm{mT}$ field where the shift is big enough to be measurable. We should then consider the fact that the g factor is a tensor, change the direction of the electric field and add the classical Stark shift in the effective hamiltonian. The incertitude of the magnetic field chosen was maybe a bit pessimistic, we plan to redo the numerical calculations with $\frac{\Delta B}{B} = 10^{-9}$.

5.2 Personal review

I was delighted to work on the EDMMA project for a further measurement of the electric dipole moment of the electron and the anapole moment of nucleus. This internship taught me a lot on how is the work of a researcher and reinforce my will to do research. It allows me also to learn new theoretical concept and to use a numerical language (Mathematica) that I never used before. I had also the opportunity to understand and work on systems that reach cryogenic temperatures.
I attended the seminars which were organized every Tuesday in the lab, and the MFC group meeting every Friday to discuss about the bibliography and to attend the presentations of other intern student. I appreciate all the fruitful discussion with my supervisors Daniel Comparat and Sebastian Lahs and with others members.

References

[1] Thomas Battard, Sebastian Lahs, Claudine Crépin, and Daniel Comparat. Cesium atoms in cryogenic argon matrix. *arXiv preprint arXiv:2305.11947*, 2023.

[2] C Crepin-Gilbert and A Tramer. Photophysics of metal atoms in rare-gas complexes, clusters and matrices. *International Reviews in Physical Chemistry*, 18(4):485–556, 1999.

[3] J Pascale and J Vandeplanque. Excited molecular terms of the alkali-rare gas atom pairs. *The Journal of Chemical Physics*, 60(6):2278–2289, 1974.

[4] L Blank, David E Weeks, and Gary S Kedziora. M+ ng potential energy curves including spin-orbit coupling for m= k, rb, cs and ng= he, ne, ar. *The Journal of Chemical Physics*, 136(12):124315, 2012.

[5] Takanori Kobayashi, Kenta Yuki, and Leo Matsuoka. An ab initio study on four low-lying electronic potential energy curves for atomic cesium and rare gas pairs. *Chemistry Letters*, 45(12):1400–1402, 2016.

[6] J Darby Hewitt, Christopher Campbell, Kyle T Raymond, Sehyun Park, Kavita V Desai, Andrey E Mironov, and J Gary Eden. Csar, csxe, and rbxe b2σ1/2+ interatomic potentials determined from absorption spectra and calculations of franck–condon factors for free–free optical transitions of atomic collision pairs. *The Journal of Physical Chemistry A*, 127(16):3675–3683, 2023.

[7] Marie-Anne Bouchiat and Claude Bouchiat. An atomic linear stark shift violating p but not t arising from the electroweak nuclear anapole moment. *The European Physical Journal D-Atomic, Molecular, Optical and Plasma Physics*, 15(1):5–18, 2001.